RESEARCH ARTICLE

Laser-based measurements and analyses on cycle-to-cycle variations of mixture formation in binary-component fuel sprays

Wenyuan Qi[1] · Yifan Zhou[1] · Yuyin Zhang[1]

Abstract

The cyclic variations of vapor distributions of a binary-component fuel spray were experimentally investigated. Ultraviolet–visible laser absorption/scattering technique was adopted for quantitative measurement of vapor mass distributions in a binary-component fuel spray. *n*-Hexane and *p*-xylene were chosen to form the binary-component test fuel. Intersection-over-union, an important concept in object detection, was firstly introduced to characterize more precisely the spray cyclic variations, in comparison with other traditional methods including presence probability image and coefficient of variation in spray penetration. As a result, a larger fluctuation was observed in vapor distributions of the higher boiling point component (*p*-xylene) in the binary-component fuel compared to that of the pure *p*-xylene spray, indicating that evaporation characteristic of multi-component fuel spray is one of the significant factors that affects the cyclic variations. Based on large amount of experimental observations, a concept of spray vapor distribution area with consideration of cyclic variation was proposed to give a more reasonable expression of spray structure, and a new empirical formula of spray vapor distribution area was given for prediction and numerical model validation.

Graphic abstract
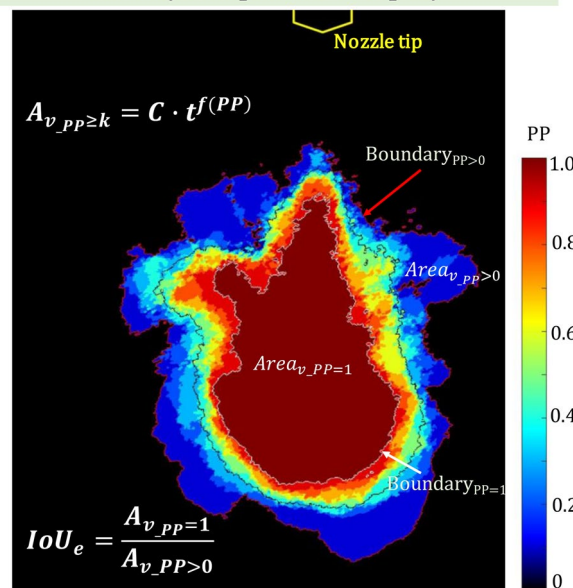
✉ Yuyin Zhang
   yuyinzhang@sjtu.edu.cn

Extended author information available on the last page of the article

1 Introduction

Providing a stable and repeatable fuel–air mixture distributions from cycle to cycle is essential to reliable ignitions and stable combustion for an internal combustion engine, as large spray variations may lead to misfire, incomplete combustion, unstable power output, low thermal efficiency and so on. However, fuel sprays are usually formed by a fuel injection from small orifices of a nozzle at high pressure, thus intrinsically stochastic in character due to the breakup processes of the instable liquid jet or liquid sheet and the subsequently induced turbulent flow around (Fansler and Parrish 2015). Hence, it is of significance to investigate the fuel spray stochastic cycle-to-cycle variation (CCV) in view of engine combustion control.

Some investigations on the fuel spray CCV have been conducted using both numerical simulation and experimental methods. Numerically, large Eddy simulation (LES) was used to analyze CCV characteristics of air–fuel mixing (Goryntsev et al. 2009, 2012) and combustion (Vermorel et al. 2009) processes in internal combustion (IC) engines. Experimentally, optical diagnostics were applied widely in the study of spray CCV, for instance, Mie scattering imaging technique for visualizing CCV characteristics of the liquid phase combining with such statistical methods as presence probability image (PPI) (Hung et al. 2003), root mean square (RMS) images (Marchi et al. 2010), proper orthogonal decomposition (POD) technique (Chen et al. 2013; Qin et al. 2015). Besides the liquid phase, CCV of the vapor distribution is also or even more important for the combustion stability as the droplets evaporation and fuel/air mixing processes are directly related to the combustion variations (Zhang and Sick 2007). Wieske et al. (2006) focused on a detailed experimental analysis of the origin of cyclic fluctuations in a spark-ignited direct-injection (SIDI) engine with an air-guided combustion process by laser-induced exciplex fluorescence (LIEF) technique. The result indicated that no obvious CCV for liquid phase but significant CCV for vapor phase flow field in their investigated operation point. Fujikawa et al. (2003) measured the fuel mixture distribution at a time of spark by planar laser-induced fluorescence (PLIF) technique, and their results suggested that the CCV of combustion was dominated by the fuel vapor concentration variations at the spark position. Wu et al. (2016) investigated the CCV characteristics of both liquid and vapor phase distributions under various superheated conditions using LIEF.

As an experimental diagnostic, LIF/LIEF technique was mostly used for detecting CCV of the vapor distribution of single-component fuel as mentioned in the above researches. For a multi-component fuel, however, it is difficult to evaluate CCV of the vapor distribution by mean of LIF/LIEF due to its complexity in distinguishing the vapor concentration distributions of different fuel components when droplets existing. However, the cyclic variations of single- and multi-component fuel are different. On the one hand, the physical properties of different components will lead to different variation characteristics (Zhang and Sick 2007; Zigan et al. 2013). On the other hand, the vapor phase variations in multi-component fuel spray may be more serious, because preferential evaporations, which often occur between different components, usually lead to a spatial stratification of different component vapor phase. Phenomenon of spatial stratification in multi-component fuel spray has been observed in many experiments (Yoon et al. 2009; Itani et al. 2015; Qi and Zhang 2019). This cyclic variation of the vapor distribution in multi-component will have important effects on ignition and flame kernel formation processes. For example, a spark-controlled compression ignition (SPCCI) gasoline engine developed by Mazda recently can be ignited and operated smoothly at an extremely lean fuel–air mixture (Gitlin 2018). Actually, an accurate and stable formation of multi-component fuel (gasoline) vapor–air mixture is one of the most essential factors for realizing the precise control of timing and position of the two ignition modes in a SPCCI engine. However, few quantitative investigations have been reported on CCV of vapor distribution in multi-component sprays. What impacts the spatial stratification of multi-component will have on CCV of vapor distribution is not clear yet.

A powerful laser diagnostic, which can realize measurement of vapor phase distribution in a multi-component spray, is necessary for the investigations of CCV of vapor phase in multi-component fuel spray. Ultraviolet–visible laser absorption/scattering (UV-LAS) technique has been proved to be effective to obtain quantitative evaporation characteristics of a binary-component fuel spray (Zhang and Nishida 2007; Qi and Zhang 2019; Chen et al. 2019). UV-LAS owns several advantages such as no oxygen-quenching, no crosstalk in signals from liquid and vapor phases and from the different tracers, lower laser energy requirement over a multi-tracer LIF/LIEF system for observation of multi-component fuel spray.

In this study, a binary-component fuel was prepared using *p*-xylene and *n*-hexane, representing the higher and the lower boiling points, respectively. CCV of the binary-component fuel spray was investigated through a UV-LAS system, which is capable of detecting the vapor distributions in a droplet-laden spray, in comparison with that of the pure *p*-xylene spray. CCV was evaluated by three statistical methods including presence probability image (PPI), coefficient of variation (COV), and Intersection-over-union (IoU). Based on CCV characteristics of the vapor distributions, a new empirical formula of spray vapor distribution

area, characterizing the spray structure of vapor phase, was proposed to give more detailed depiction of a spray besides the spray penetration and angle.

2 Experimental setup and conditions

2.1 Principle of UV-LAS technique

UV-LAS technique consists of two wavelength light channels: a visible channel (transparent wavelength, $\lambda_T = 532$ nm) to obtain the droplets optical thickness and an ultraviolet channel (absorption wavelength, $\lambda_a = 266$ nm) to obtain the optical thickness of both vapor and droplets, which are based on the absorption and scattering of fuel vapor and droplets in a spray. UV-LAS imaging system as well as other related experiment apparatus are shown in Fig. 1. In the measurement, the incident light with intensity of I_0 will turn into I_t due to the extinction of absorption and scattering. The extinction of visible light is from the scattering of droplets, while the extinction of ultraviolet light is resulting from both the vapor absorption and droplets absorption and scattering. The extinction of two wavelength can be expressed based on the Lambert–Beer's law and the scattering theory of small particles as follows (Zhang 2001):

$$\log(I_0/I_T)_{\lambda_a} = \int_0^L \varepsilon_{\lambda_a} \cdot C_{v(x)} \mathrm{d}x + \int_0^L K^{\mathrm{ext}}_{\lambda_a} \mathrm{d}x, \tag{1}$$

$$\log(I_0/I_T)_{\lambda_T} = \int_0^L K^{\mathrm{ext}}_{\lambda_T} \mathrm{d}x, \tag{2}$$

where I_0 is the intensity of incident light, I_T is the intensity of transmitted light, $\varepsilon_{\lambda a}$ (l cm^{-1} mol^{-1}) is the molar absorption coefficient (MAC) of fuel vapor at λ_a, $C_{v(x)}$ is the vapor concentration (mol m^{-3}) at position x, L is the optical path length (m), $K^{\mathrm{ext}}_{\lambda_a}$, $K^{\mathrm{ext}}_{\lambda_T}$ are the extinction coefficient (m^{-1}) for a cloud of droplets at the two wavelengths.

The line-of-sight-averaged fuel vapor concentration $\overline{C}_v$ will be obtained from Eqs. (1) and (2):

$$\overline{C}_v = \frac{1}{\varepsilon_{\lambda_a} \cdot L} \cdot \log(I_0/I_T)_{\lambda_a} - R \cdot \log(I_0/I_T)_{\lambda_T}, \tag{3}$$

where R is the ratio of the droplets optical thickness at the two wavelengths (λ_a and λ_T) and defined as the following equation:

$$R = \left. \frac{\int_0^L K^{\mathrm{ext}}_{\lambda_a} \mathrm{d}x}{\int_0^L K^{\mathrm{ext}}_{\lambda_T} \mathrm{d}x} \right|_{\mathrm{droplet}} \approx 1. \tag{4}$$

In fact, it has been experimentally confirmed that the ratio of optical thickness of droplets in a typical fuel spray, R, approaches to 1, if the half-detection angles are designed differently to eliminate the effect of wavelength on droplets scattering (Zhang 2001; Pastor et al. 2016). The assumption can lead to some bias in the area where the liquid phase is dominated of fuel spray. In this paper, the attention was focused on the vapor phase when droplets have evaporated sufficiently. The assumption of $R = 1$ will cause little bias.

Fuel vapor concentration distributions in the projected plane along the line-of-sight can be obtained through Eq. (4),

$$M_v = \overline{C}_v \cdot L = \frac{1}{\varepsilon(\lambda_a)} \left[\log\left(I_0/I_T\right)_{\lambda_a} - R \cdot \log\left(I_0/I_T\right)_{\lambda_T} \right]. \tag{5}$$

It is worth noting that $\varepsilon(\lambda_a)$ always depends on mixture temperature. In this study, to reduce the effect of temperature on concentration measurement accuracy, the mixture temperature was predicted based on a thermal energy

Fig. 1 Setup of UV-LAS imaging system
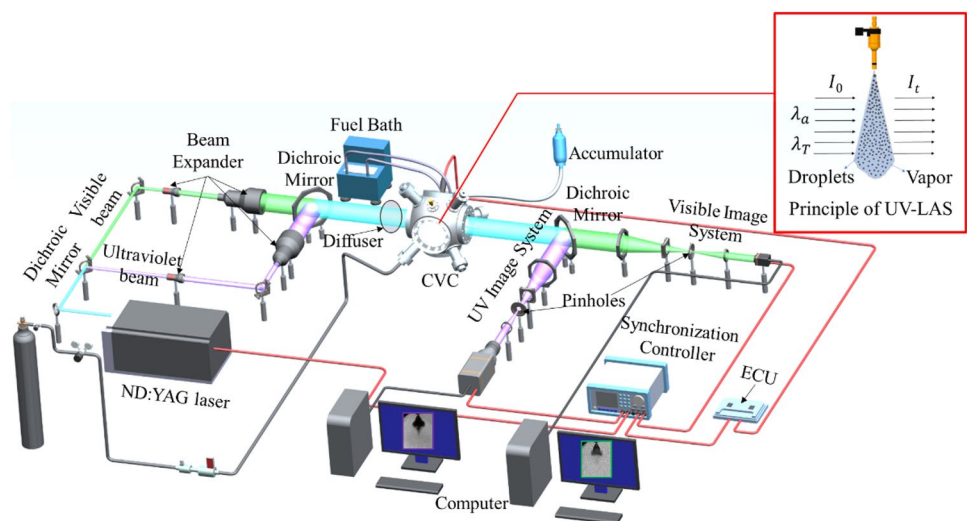
conservation model (Senda et al 1997; Zhang 2001) and the corresponding concentration was corrected. The detailed depictions of the UV-LAS principle and the processing method are referred to the previous publications (Zhang 2001). The measurement error is with 10% for vapor concentration in a binary-component fuel spray (Qi and Zhang 2019).

2.2 Experimental setup

A scavenging spherical constant volume chamber (SCVC) system (Fig. 1) was developed to simulate the thermodynamic conditions for measurement of vapor concentration distributions of single- and binary-component fuel spray. The SCVC system allows to maintain conditions at maximum pressure of 6 MPa and 900 K maximum temperature. The test section of the SCVC system has four windows (100 mm in diameter) positioned at a 90°, and two of them at 180° were used for line of sight measurement in this work. The working process of SCVC system was similar to a constant pressure flow (CPF) test rig in CMT and Caterpillar mentioned in Meijer et al. (2012). During the process of SCVC system operation, pressurized nitrogen gas passed through electrical heaters. The gas temperature was easily, precisely, and automatically controlled by a volt controller. The gas pressure was controlled through a PID system and an electric backpressure valve. When SCVC system was under steady conditions, the deviation of temperature and pressure in test area is less than ca. 1%, respectively. To obtain a uniform temperature field, the heated gas entered into the test area of SCVC from three center-oriented inlets, and internal walls with thermal insulation material were installed near the outer stainless steel walls.

A Nd:YAG laser (Spectra-Physics, LAB-150-10H) provided a light beam including wavelengths of 266 nm and 532 nm. A dichroic mirror was used to separate the two beams, an ultraviolet beam ($\lambda_a = 266$ nm) and a visible beam ($\lambda_T = 532$ nm), which were then expanded to a diameter of 100 mm, respectively. Effect of beam steering was eliminated by a specific diffuser installed after beam expanders (Westlye et al. 2017). After passing through the fuel spray in chamber, the beams were re-separated into two channels. Finally, an ICCD camera (Andor, DH334T-18H-83)

equipped with collimating lenses was adopted to collect the ultraviolet images, and a CCD camera (Imperx, B1620) was used for visible image collection. Bandpass filters (Edmund, 266 nm and 532 nm) were installed before cameras to avoid spectral interference of two wavelength. The detailed depictions about the experimental setup are referred to our previous paper (Qi and Zhang 2019).

2.3 Test fuels

n-Hexane and *p*-xylene, both of which exist in the commercial gasoline, were chosen to form the test binary-component fuel (written as *n*-hex/*p*-xy) in molar ratio of 1:1, where *n*-hexane represents the low boiling point (LBP) component and *p*-xylene represents the high boiling point (HBP) component. Some physical properties of the two components are given in Table 1. It should be noted that *p*-xylene has strong absorption at wavelength of 266 nm, while *n*-hexane shows scarce absorption at wavelength of 266 nm. So, the vapor mass concentration of *p*-xylene in a binary-component fuel *n*-hex/*p*-xy can be detected using UV-LAS technique (Qi and Zhang 2019).

2.4 Experimental conditions

The experimental conditions are listed in Table 2. The temperature was set at 623 K and pressure was set at 0.45 MPa which approached the typical environment in cylinder during fuel injection process for a turbo-charged gasoline engine. A swirl injector was adopted in this study.

Table 2 Experimental conditions

Items	Specification
Injector type	Swirl
Ambient gas	Nitrogen
Ambient pressure (P_a)	0.45 MPa
Ambient temperature (T_a)	623 K
Test fuel	*p*-Xylene, *n*-hex/*p*-xy
Injection pressure (P_{inj})	3 MPa
Injection duration (Δt_{inj})	1.0 ms
Fuel temperature (T_f)	323 K

Table 1 Thermal-physical properties of test fuels (Zigan et al. 2011; Qi and Zhang 2019)

	Unit	*n*-Hexane	*p*-Xylene	Fluorobenzene	Gasoline
Molecular weight	g mol^{-1}	86.2	106.2	96.1	–
Boiling point	K	341.7	411.4	358.0	308–473
Density	kg m^{-3}	656	857	1020	720–740
Surface tension	mN m^{-1}	17.9	27.9	27.4	22
Kinematic viscosity	m^2 s^{-1}	0.446	0.706	0.566	0.530
Vaporiz. heat	MJ kmol	31.5	42.2	34.6	–

# 3 Image processing and statistical methods

3.1 Image processing

The image process flowchart of UV-LAS is shown in Fig. 2. Two pairs of images including ultraviolet light (λ_a) and visible light (λ_T) channel were obtained from cameras in UV-LAS technique. $\log(I_0/I_T)_\lambda$ was applied for raw extinction images to obtain the optical thickness of two wavelengths in Eqs. (1) and (2). This step also eliminated the fluctuation of laser pulse by energy confirmation in a zone (100×100 pixels) background images away from the spray area both in raw extinction images and background images. Vapor mass concentration was then obtained by Eq. (5) combined with temperature correction and $\varepsilon(\lambda_a)$. The detailed description of $\varepsilon(\lambda_a)$ calibration can be referred to the previous paper (Qi and Zhang 2018, 2019).

3.2 PPI method

Presence probability image (PPI) method was adopted in this paper to characterize the CCV of vapor distributions. The algorithm for determination of the PPI was shown briefly in Fig. 2. Firstly, the region of spray vapor phase presence in each image was identified based on thresholding technique. The determination of threshold was referred to SAE standard (Hung et al. 2008). The histogram of image intensity usually exhibits two peaks: one represents the background pixels and the other represents the spray image pixels. An appropriate threshold for separating the spray domain from the background can be obtained according to the maximum between-cluster variance principle (Otsu 1979). The practical threshold was approximately 2.2–2.4% of the dynamic range of the CCD camera (16 bit) in this work.

So, the vapor concentration images changed to the binary images where the value of spray vapor phase region was 1 (white pixel) and the value of remaining region was 0 (black pixel). Secondly, all binary images were added up pixel-by-pixel and then were divided by the total number of images to

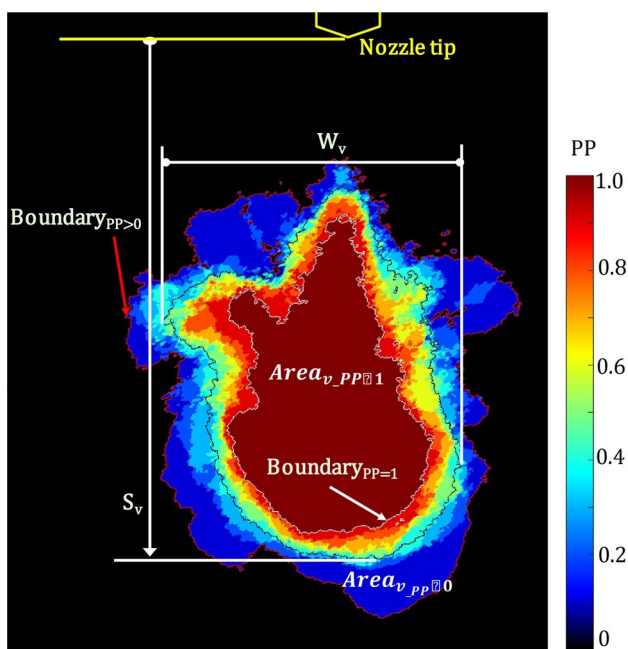**Fig. 2** Image process flowchart of UV-LAS imaging technique and PPI method
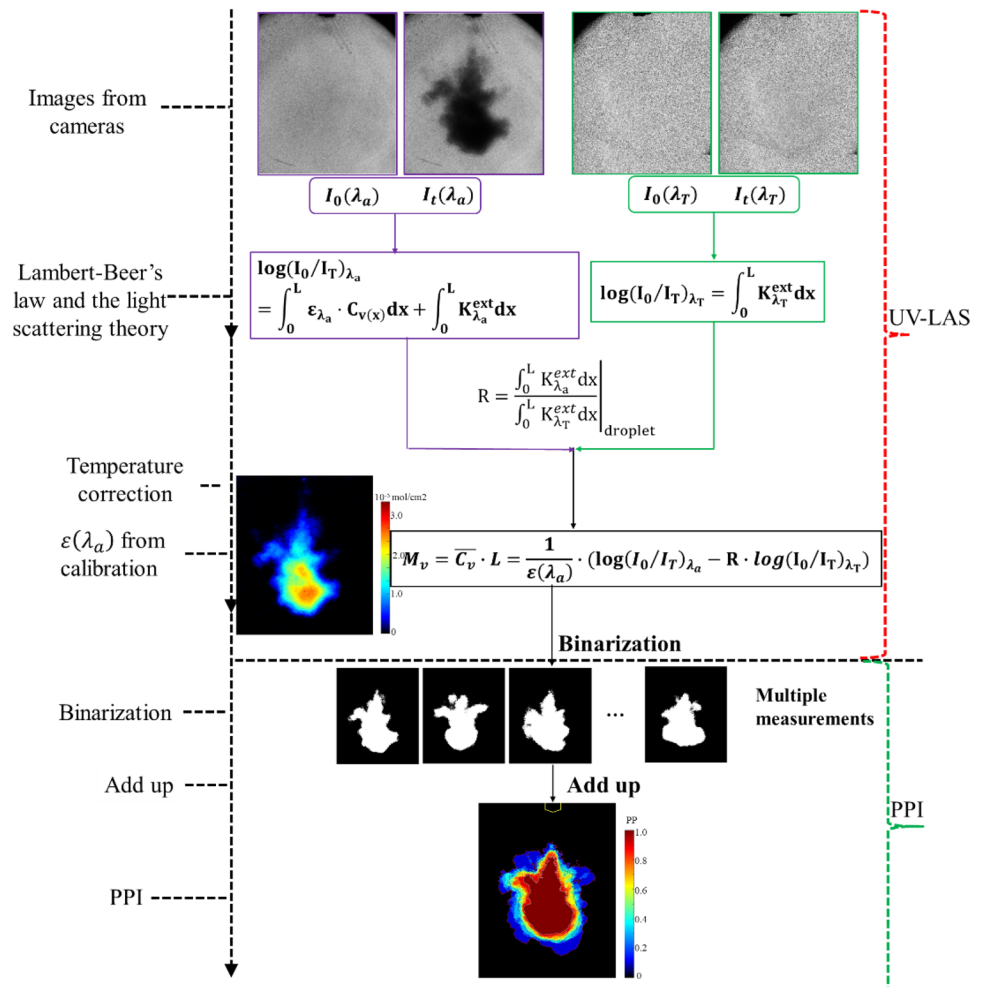
Fig. 3 PPI and definition of macrostructure of fuel vapor phase

Fig. 4 Schematic of IoU calculation

form PPI of vapor distributions (Fig. 3). Finally, the value of each pixel corresponds to the vapor presence probability (PP) at its location. For example, the value of 0.9 means vapor presence probability is 90%. More details about the PPI algorithm can refer to the publication before (Hung et al. 2003).

In order to facilitate the following study and analysis on the CCV characteristics, some parameters to represent the macrostructure of spray vapor phase were defined based on PPI. As shown in Fig. 3, the spray vapor PPI boundary ($Boundary_{pp \geq k}$) was extracted if the value of PPI is equal to or larger than k. In particular, $Boundary_{pp>0}$ means the total area boundaries of fuel vapor phase in all images. $Boundary_{pp=1}$ means complete overlap area boundary of the vapor phase in all images. The area through the $Boundary_{pp \geq k}$ was written as $A_{v\_PP \geq k}$. Vapor penetration was defined as the longest distance that the spray travelled in the vertical direction from the nozzle tip to the spray boundary.

3.3 Definition of Intersection-over-union (IoU)

Intersection-over-union (IoU) was introduced here to characterize the variations of fuel spray. IoU is an important concept (also known as Jaccard index) which was applied wildly in the object detection. The IoU of area A and area B (shown in Fig. 4) can be expressed as:

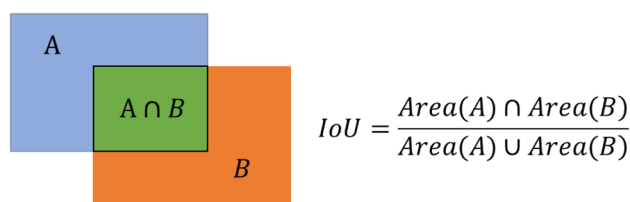$$IoU = \frac{Area(A) \cap Area(B)}{Area(A) \cup Area(B)}. \tag{6}$$

The value of IoU ranges from 0 to 1. When A and B are completely coincident, the value of IoU is 1. If there is no intersection between A and B, IoU equals 0. The smaller the IoU, the greater the difference between A and B.

Multiple spray areas need to be dealt with in the analysis of spray cyclic variations, and the extended IoU_e was defined as:

$$IoU_e = \frac{Area\left(spray_1\right) \cap Area\left(spray_2\right) \cap \cdots \cap Area\left(spray_n\right)}{Area\left(spray_1\right) \cup Area\left(spray_2\right) \cup \cdots \cup Area\left(spray_n\right)}. \tag{7}$$

The IoU_e can also be expressed as follows:

$$IoU_e = \frac{A_{v\_PP=1}}{A_{v\_PP>0}} \tag{8}$$

where $A_{v\_PP>0}$ is the total area of spray vapor and $A_{v\_PP=1}$ is the complete overlap area in PPI, which were defined in Sect. 3.2.

4 Results and discussion

Multiple measurements are required for analysis of CCV of a fuel spray. In order to determine the appropriate number of measurements for evaluating CCV, the measurement at the same conditions was repeated 30 times. Figure 5 gives IoU_e of the vapor phase in a spray at 1.0 ms after start of fuel (ASOF) with various cycle number. As shown in Fig. 5, IoU_e reduced 15% when the number of cycles increased from 5 to 30. It is reasonable to set the number of cycles to 10 for investigating CCV of fuel vapor distribution as IoU_e varied only 7% when the number of cycles increased from 10 to 30.

4.1 Evaporation characteristics of binary-component fuel spray

Quantitative fuel vapor mass distributions (mol cm^{-2}) of pure p-xylene and p-xylene in p-xy/n-hex binary component were attained by UV-LAS technique, and the results were shown in Fig. 6. The measurement error of vapor mass distributions was less than 8.07%. The detailed measurement
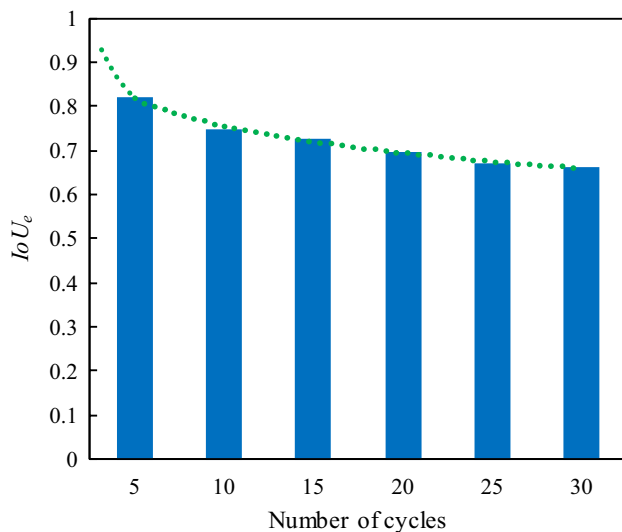
Fig. 5 IoU_e of fuel vapor distribution with various cycle number ($T_a = 623$ K, $P_{inj} = 3$ MPa, $P_a = 0.45$ MPa, $\Delta t_{inj} = 1.0$ ms, $t_{ASOF} = 1.0$ ms)

accuracy analysis can be referred to our previous paper (Qi and Zhang 2019).

As shown in Fig. 6, the raw images (single-shot data) at the two wavelengths (UV. and Vis.) were listed in pairs with the vapor mass distribution image (single- and 10-times averaged data) right below them for different shot timings. It was obvious that at the moment of $t_{ASOF} = 1$ ms (during injection), both spray images of pure p-xylene and p-xylene in the binary component look similar for either cases of liquid phase or vapor phase, indicating that difference in atomization characteristics resulting from the fuel properties of pure p-xylene or p-xylene in the binary component was quite small during injection in this work. In contrast, after end of injection ($t_{ASOF} = 2$–3 ms) there was significant difference in vapor mass distributions between pure p-xylene and p-xylene in the binary components, and the liquid phase almost disappeared.

In order to examine the effect of one component on the evaporation of the other component in a binary-component fuel spray, the mass of the evaporated LBP (Fluorobenzene) and HBP (p-xylene) components in the binary-component fuel under the same operating conditions was measured using UV-LAS technique with component substitution. In the measurement, in order to obtain the evaporation characteristics of LBP component (n-hexane), absorbing component fluorobenzene was selected as the substitution component of n-hexane combined with a non-absorbing component n-octane to form another binary-component fuel. The vapor mass distribution and evaporated mass of LBP component (Fluorobenzene) can be obtain using UV-LAS technique. Fluorobenzene was used to substitute the n-hexane

completely, and the comparison of their thermal-physical properties is shown in Table 1. Validation of the reasonability of components substitution method and more detailed descriptions of the measurement method can be referred to our previous paper (Qi and Zhang 2019). The ratio of the evaporated mass (molar) of LBP and HBP components was obtained and shown in Fig. 7. The results were the average of 10 times measurement. The vapor mass ratio of LBP to HBP increases gradually with t_{ASOF} from 1 to 4 ms, indicating that LBP evaporated faster than HBP. The vapor mass ratio approaches to 1 when $t_{ASOF} \geq 4$ ms, indicating that both LBP and HBP have evaporated completely at/after this moment. This fact supported that the preferential evaporation in the binary-component fuel spray occurred under this operating condition. Preferential evaporation would occur during evaporating process ($t_{ASOF} < 4$ ms), and then, components would mix again after both components evaporated completely ($t_{ASOF} \geq 4$ ms) due to the effect of air entrainment and dilution.

4.2 Cyclic variations in vapor phase distributions in the binary-component spray

PPIs of p-xylene vapor distributions in the binary-component spray compared to those in the pure p-xylene spray at different shot timings are shown in Fig. 8. It was obvious that the cyclic variations of p-xylene vapor distribution in the binary-component spray and in the pure p-xylene spray became serious with time after start of fuel (t_{ASOF}). The small fluctuations were observed only in the vicinity of the leading edge of the spray during injection ($t_{ASOF} = 1$ ms), to which similar trend can be also found in the previous report (Hung et al. 2003), indicating that variation in spray characteristics due to atomization effects of different fuel components was small. After end of injection ($t_{ASOF} > 1$ ms), the conspicuous fluctuations appeared gradually at both left and right sides of the spray, which was also observed by Rayleigh scattering measurements (Schulz et al. 2004). From Fig. 8, it seems that the cyclic variations of p-xylene vapor distributions in the binary-component spray were slightly larger than those in the pure p-xylene spray, but the difference in-between was not so significant. So, it is difficult to distinguish the CCV differences between pure- and binary-component fuel spray quantitatively using PPI results.

In this circumstance, coefficients of variation (COV) of the spray vapor penetration and width were adopted to evaluate CCV. As shown in Fig. 9, the penetrations of p-xylene vapor in the binary-component spray were slightly larger than those in the pure p-xylene spray. However, the differences in cyclic variation between pure p-xylene spray and the binary-component are not noticeable in the perspective of COV of vapor penetration.

Fig. 6 Raw single-shot images (extinction) of UV and VIS and images of vapor mass distribution (mol cm^{-2}) for pure p-xylene spray and p-xylene in p-xy/n-hex binary-components fuel sprays at 1.0, 2.0, 3.0 ms ASOF ($T_a = 623$ K, $P_{inj} = 3.0$ MPa, $P_a = 0.45$ MPa, $\Delta t_{inj} = 1.0$ ms)
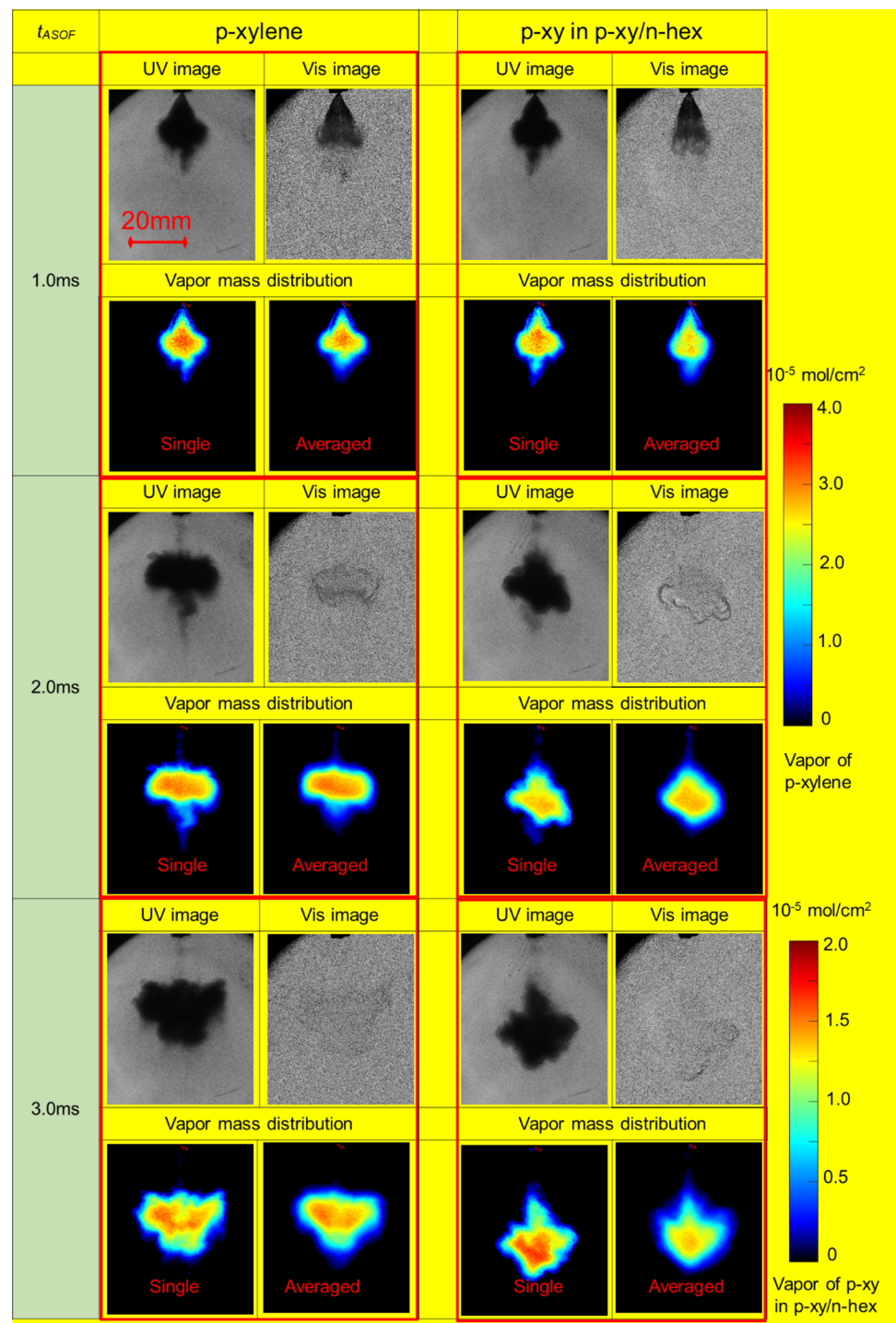
Meanwhile, as shown in Fig. 10, the spray width of p-xylene vapor in the binary-component was slightly less than that in the pure p-xylene. COV of spray width of p-xylene vapor in the binary-component was larger than that of pure p-xylene, indicating that the cyclic variations of p-xylene vapor in the binary-component fuel spray was greater.

It should be noted that the spray penetration or width only represents a distance of spray structure, although they are commonly used for characterizing spray macrostructure and simulation validation. It is quite difficult to characterize CCV of spray vapor distributions comprehensively by use of deviation in spray penetration and width, because COV of penetration or width only represents the variation of
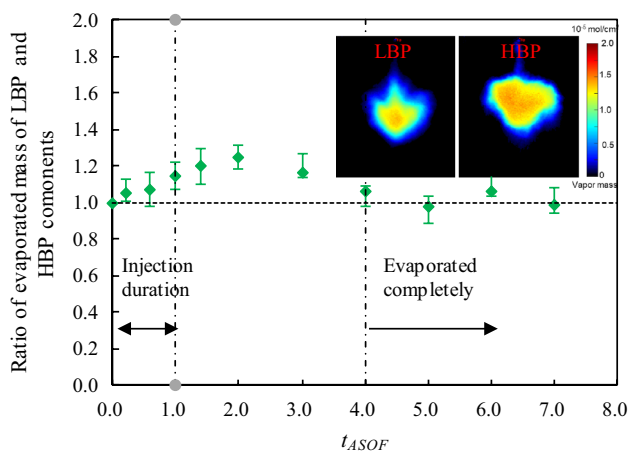
Fig. 7 Ratio of evaporated mass of LBP (fluorobenzene) and HBP (*p*-xylene) components vs. time after start of fuel (t_{ASOF}) in the binary-component fuel spray under conditions: $T_a = 623$ K, $P_{inj} = 3.0$ MPa, $P_a = 0.45$ MPa, $\Delta t_{inj} = 1.0$ ms

distance dimensions in one direction. Instead, IoU_e, which depends on both the position and shape of a spray, not only on the distance from nozzle as defined in Sect. 3.3, could be more preferable and appropriate than penetration COV or deviation when characterizing CCV of vapor distributions in a spray.

Based on a series of measurements, IoU_e of *p*-xylene vapor distributions in the pure *p*-xylene spray and in the binary-component spray is summarized in Fig. 11. The results of IoU_e provide an explicit value to evaluate the degree of cyclic variation of a spray, so it is clearer and more quantitative than PPI (as shown in Fig. 8) when used to compare the cyclic variation differences of *p*-xylene vapor distribution in the pure *p*-xylene and in the binary-component spray. It is obvious that IoU_e of the *p*-xylene vapor distributions in the pure *p*-xylene spray is significantly smaller compared to that in the binary-component spray, indicating that the cyclic variation of *p*-xylene vapor in the binary-component spray is larger than that of pure *p*-xylene. This is an evidence that the vapor distribution of HBP component (*p*-xylene) in the binary-component spray has been influenced by the other LBP component (*n*-hexane), which was called the preferential evaporation in multi-component fuel, i.e., the vapor phase of HBP component preferentially located in the far-field (Yoon et al. 2009) or the vortex core (Itani et al. 2015) of the spray where fluctuations occurred more likely. This finding revealed that the preferential evaporation and spatial stratification in a binary-component spray will have an important effect on the mixing process and lead to different fluctuation degrees between single- and multi-component fuel.

The analysis on fuel vapor cyclic variations can be divided into two stages (see Fig. 11): during injection and

after end of injection. In the first stage, less change in IoU_e occurs, and the spray concentrated in the axial area due to the momentum of injection which kept the jet (spray) stable. Cyclic variations of vapor distributions of both pure *p*-xylene and *p*-xylene in binary-component fuel are not significant during injection, when the variations were dominated by the inertia force of injection and atomization effect. This result is consistent with that in other literature that no obvious CCV for liquid phase occurs (Wieske et al. 2006; Hung et al. 2003). In the second stage, IoU_e declines rapidly with time, indicating that the stabilities of the jet (spray) got worse. The inertia force in the injection direction became weak and did not play the leading role any more after the end of injection; thus, the vapor phase dispersed all around due to spray-induced vortex and air entrainment. As shown in Fig. 12, the differences in penetration speed and width expansion ($D_{sp} = $ Speed$_{penetration} - $ Speed$_{width}$) of *p*-xylene vapor both in the pure *p*-xylene and in the binary-component spray decrease with increase of t_{ASOF} during injection, while the value of D_{sp} remains stable after end of injection ($t_{ASOF} \geq 2$ ms). These results also indicate that the moment that the fuel injection ends is an important turning point: During injection (the first stage) the inertia force (the fuel injection) plays a dominated role, but after end of injection (the second stage) the diffusion and mixing into each other of fuel vapor and the ambient gas plays a dominated role on the spray development.

It is also clear from the above analysis that IoU_e can provide more insightful information than PPI and COV do when evaluating CCV of vapor distributions in a spray.

4.3 Cyclic variations of vapor distribution area

When considering cyclic variations, the area ($A_{v\_PP \geq k}$) of vapor distributions in a spray can be defined in Sect. 3.2 and illustrated in Fig. 3. The evolutions of the maximum value ($A_{v\_PP > 0}$), the minimum value ($A_{v\_PP = 1}$), and the averaged value (A_{v_ave}) of the vapor distribution area are summarized in Fig. 13, where $A_{v\_PP > 0}$ and $A_{v\_PP = 1}$ represent the union and the intersection, respectively. The fluctuations of the vapor distribution area were obviously big for both the pure *p*-xylene spray in Fig. 13a and the binary-component spray in Fig. 13b. This significant fluctuation may mislead the engine engineer when optimizing the mixture formation processes among parameters of the spray shape and position, the combustion chamber geometry, and the inner gas flow. The modeling work may also fail to find right data to validate the model due to this underestimated spray characteristics if the fluctuations are not accounted for. For example, the spray is likely to impinge on the piston or cylinder walls and even wets them as the real distribution area could be much larger at a big probability if the intersection ($A_{v\_PP = 1}$) is presumed as the right area of the
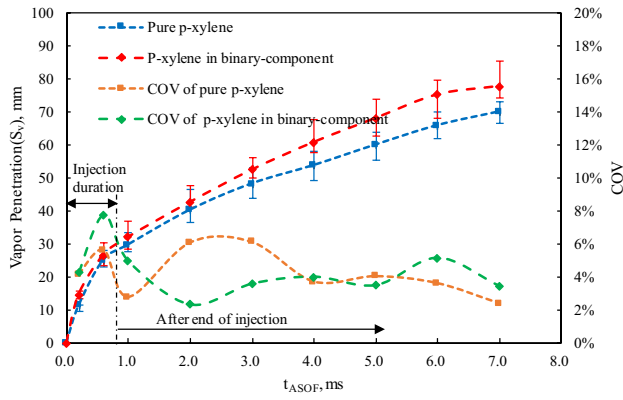
Fig. 8 PPIs of the *p*-xylene vapor distribution in the binary-component spray in comparison to those in the pure *p*-xylene spray ($T_a = 623$ K, $P_{inj} = 3$ MPa, $P_a = 0.45$ MPa, $\Delta t_{inj} = 1.0$ ms)
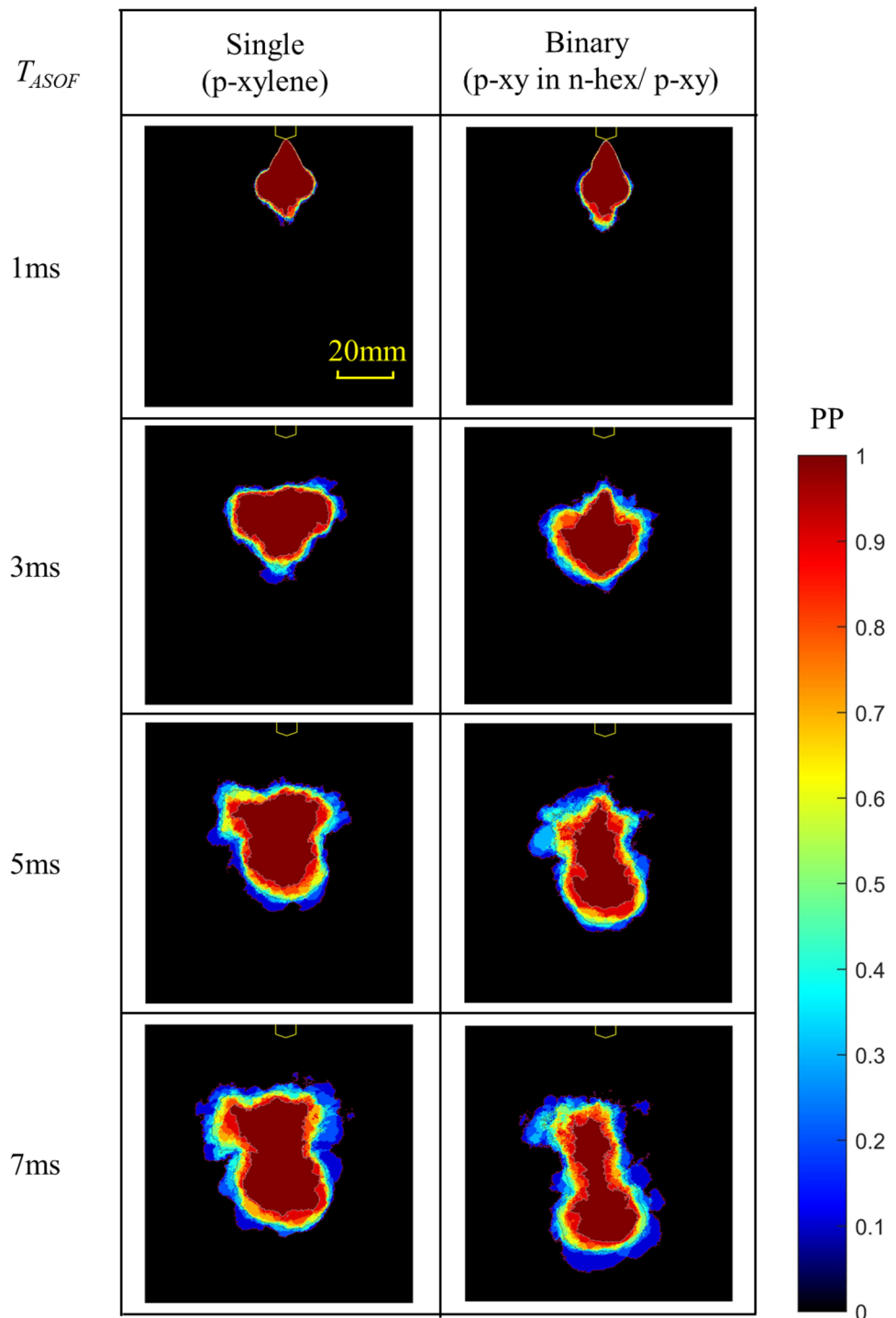

fuel distribution. The area increases with decrease of presence probability (PP). The averaged value (A_{v_ave}) could be a compromised choice, but the union ($A_{v\_PP>0}$) may be the best choice for judgment of fuel spray impingement problem. However, the union is not always the best choice as it is the biggest one and thus likely overestimated. The averaged value is usually preferred for calibration or validation of a RANS simulation model, while the intersection can be used to find the right position of spark plug so as to ensure that the vapor/air ratio is proper for ignition at all circumstances. It is clear that the new definition of spray vapor distribution area considering cyclic variation is helpful in various ways related to optimization of engine combustion system.

It is interesting to find that the fitting curve of the vapor distribution area ($A_{v\_PP \geq k}$), which increases with time after
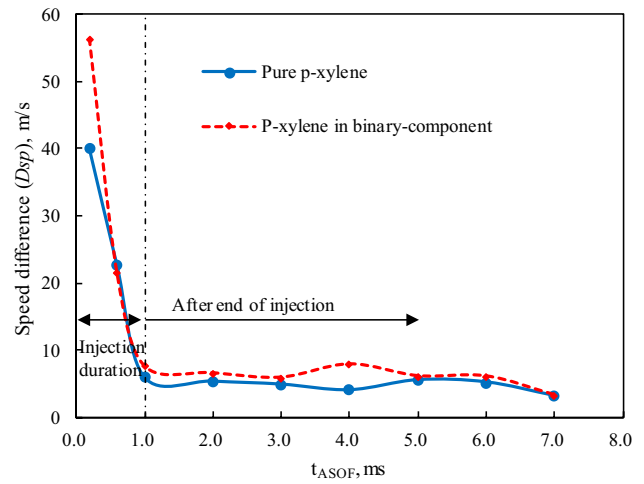
Fig. 9 Deviation of *p*-xylene vapor penetration (S_v) and their COVs in the pure *p*-xylene spray and in the binary-component fuel spray ($T_a = 623$ K, $P_{inj} = 3.0$ MPa, $P_a = 0.45$ MPa, $\Delta t_{inj} = 1.0$ ms)
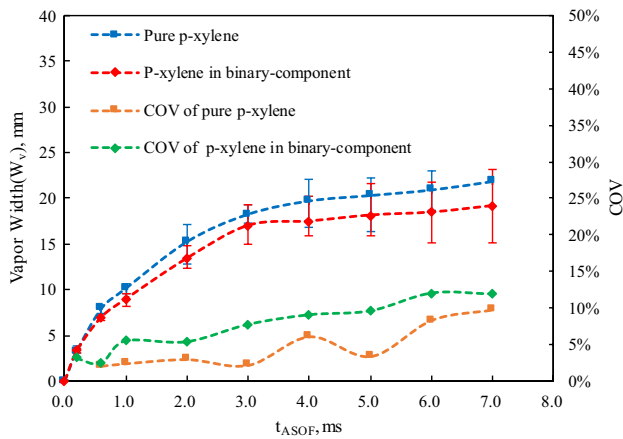

Fig. 10 Deviation of spray width of *p*-xylene vapor (W_v) and their COVs in the pure *p*-xylene spray and in the binary-component fuel spray ($T_a = 623$ K, $P_{inj} = 3.0$ MPa, $P_a = 0.45$ MPa, $\Delta t_{inj} = 1.0$ ms)
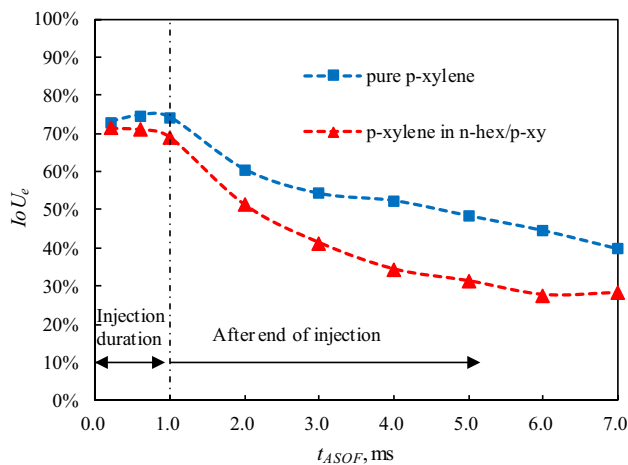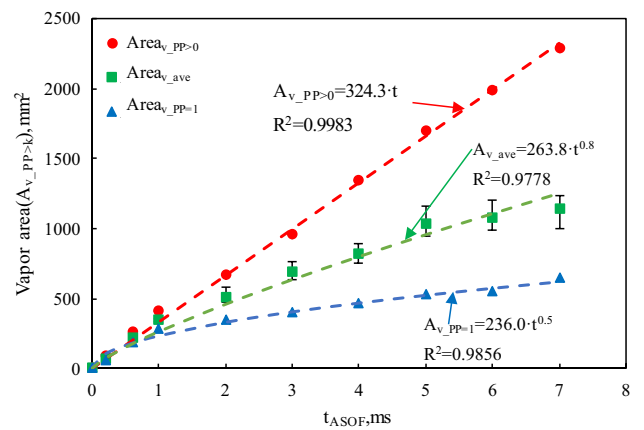

Fig. 11 IoU$_e$ evolutions of *p*-xylene vapor distribution in the pure *p*-xylene spray and in the binary-component spray ($T_a = 623$ K, $P_{inj} = 3$ MPa, $P_a = 0.45$ MPa, $\Delta t_{inj} = 1.0$ ms)

Fig. 12 Differences in speed of penetration and width of *p*-xylene vapor in the pure *p*-xylene spray and binary-component spray ($T_a = 623$ K, $P_{inj} = 3.0$ MPa, $P_a = 0.45$ MPa, $\Delta t_{inj} = 1.0$ ms)
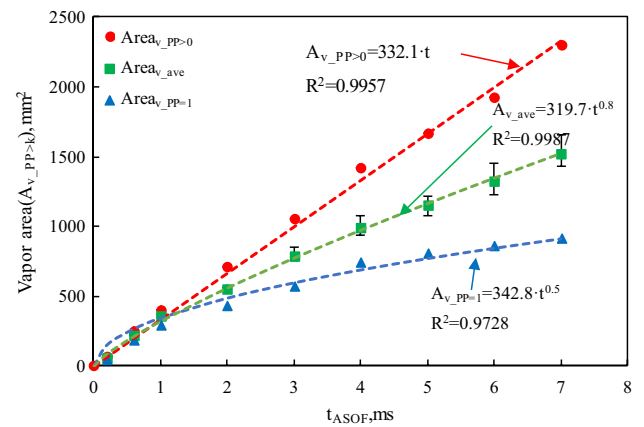
(a) In the pure p-xylene

(b) In the binary-component spray

Fig. 13 Evolution of *p*-xylene vapor distribution area ($A_{v\_PP>k}$), **a** in the pure *p*-xylene spray, **b** in the binary-component spray ($T_a = 623$ K, $P_{inj} = 3$ MPa, $P_a = 0.45$ MPa, $\Delta t_{inj} = 1.0$ ms)

start of fuel (t_{ASOF}), can be well approximated by a power function:

$$A_{v\_PP \geq k} = C \cdot t^{f(k)}, \tag{9}$$

where C is the coefficient which is related to the ambient conditions and the injection parameters, t, is the time after start of fuel (t_{ASOF}). The index $f(k)$ is related to the presence probability (PP). In the experimental condition of this paper, the $f(k)$ of the total area ($A_{v\_PP>0}$), the average area (A_{v_ave}), and the complete overlap area ($A_{v\_PP=1}$) equal to 1, 0.8, and 0.5, respectively, which are applicable to both the pure p-xylene spray and the binary-component spray (Fig. 13), that is,

$$A_{v_{pp}>0} = Ct, \tag{10}$$

$$A_{v\_ave} = Ct^{0.8}, \tag{11}$$

$$A_{v_{PP}=1} = Ct^{0.5}. \tag{12}$$

Some researchers (Hiroyasu and Arai 1990; Naber and Siebers 1996; Payri et al 2007; Zhang et al. 2017; Zhou et al 2019) proposed empirical equations to predict the macroscopic parameter of spray, such as the spray penetration, cone angle, vapor mass and so on. However, none of them considered the cyclic variations of sprays as in Eq. (9). It is important to improve these empirical equations by considering the fluctuations for better utilizing the experimental data for different purposes related on the real engine combustion optimization and model calibration/validation. For determination of a general expression including $f(k)$ in Eq. (9), further experiments under more conditions will be required.

5 Summary and conclusions

To explore the effect of preferential evaporation in multi-component fuel spray on variations of vapor distribution, ultraviolet–visible laser absorption/scattering (UV-LAS) system was established for quantitatively detecting the p-xylene vapor distributions in both the pure p-xylene spray and the binary-component (p-xylene/n-hexane) spray. Different statistical methods including Intersection-over-union (IoU), presence probability image (PPI), and coefficient of variation (COV) in penetration were proposed or adopted to facilitate the analysis on CCV. Main conclusions are as follows:

1. Intersection-over-union (IoU) was firstly introduced to characterize the variations of vapor distribution in a fuel spray. IoU was further extended to IoU_e in this paper as IoU is used for only two objectives, while there are multiple objectives to deal with in the analysis of spray cyclic variations. It was found that IoU_e is a more effective statistical method than the presence probability image (PPI) method when applied to compare the degree of cyclic variations in vapor distribution between single- and binary-component spray quantitatively. Deviation (error bar) or coefficient of variation (COV) in penetration, which are commonly used for expressing spray variation, are incapable of representing the cyclic variations of vapor distribution comprehensively. IoU_e can give such more insightful information beyond the penetration (COV) as spray penetration is only a meter of distance in the vapor distribution from injector nozzle, while IoU_e involves shape and position information of spray distribution.

2. Larger cyclic variation was observed in vapor distribution of the higher boiling point component (p-xylene) in the binary-component fuel compared to that in the pure p-xylene spray, which proved that interactions between different components (for example, spatial stratification in multi-component fuel spray) have important effects on variations in vapor distribution. This variation in vapor distribution of different components will be very helpful when optimizing the ignition process and the early flame kernel formation of an engine.

3. A new prediction equation of spray vapor distribution area was proposed to characterize the vapor phase behavior when considering cyclic variation. It was found that the total distribution area of vapor phase ($A_{v\_PP \geq k}$) can be well approximated by a power function: $A_{v\_PP \geq k} = C \cdot t^{f(k)}$, where the index $f(k)$ is related to the cyclic variation, taking the value of 0.5, 0.8, and 1.0, respectively, for the intersection ($k > 0$), the averaged ($k = 0.5$), and the union ($k = 1$) of the vapor distribution areas under the experiment conditions in this work.

References

Chen H, Hung DLS, Xu M, Zhong J (2013) Analyzing the cycle-to-cycle variations of pulsing spray characteristics by means of the proper orthogonal decomposition. At Sprays 23:623–641

Chen R, Nishida K, Shi B (2019) Quantitative investigation on the spray mixture formation for ethanol-gasoline blends via UV–Vis dual-wavelength laser absorption scattering (LAS) technique. Fuel 242:425–437

Fansler TD, Parrish SE (2015) Spray measurement technology: a review. Meas Sci Technol 26(1):012002

Fujikawa T, Nomura Y, Hattori Y, Kobayashi T, Kanda M (2003) Analysis of cycle-by-cycle variation in a direct injection gasoline

engine using a laser-induced fluorescence technique. Int J Engine Res 4:143–153

Gitlin JM (2018) Compression ignition engines are a big breakthrough—we got to try one. Ars Technica Web. https://arstechnica.com/cars/2018/01/mazdas-skyactiv-x-shows-the-internal-combustion-engine-has-a-future/

Goryntsev D, Sadiki A, Klein M, Janicka J (2009) Large eddy simulation-based analysis of the effects of cycle-to-cycle variations on air-fuel mixing in realistic DISI IC-engines. Proc Combust Ins 32(2):2759–2766

Goryntsev D, Sadiki A, Janicka J (2012) Cycle-to-cycle variations based unsteady effects on spray combustion in internal combustion engines by using LES. SAE tech paper 2012-01-0399

Hiroyasu H, Arai M (1990) Structures of fuel sprays in diesel engines. SAE tech paper 1050-1061

Hung DLS, Chmiel DM, Markle LE (2003) Application of an imaging-based diagnostic technique to quantify the fuel spray variations in a direct-injection spark-ignition engine. SAE tech paper 2003-01-0062

Hung DLS, Harrington DL, Gandhi AH et al (2008) Gasoline fuel injector spray measurement and characterization—a new SAE J2715 recommended practice. SAE Int J Fuels Lubr 1(1):534–548

Itani LM, Bruneaux G, Di Lella A, Schulz C (2015) Two-tracer LIF imaging of preferential evaporation of multi-component gasoline fuel sprays under engine conditions. Proc Combust Inst 35:2915–2922

Marchi A, Nouri J, Yan Y, Arcoumanis C (2010) Spray stability of outwards opening pintle injectors for stratified direct injection spark ignition engine operation. Int J Engine Res 11:413–437

Meijer M, Somers B, Johnson J, Naber J, Lee SY, Malbec LMC, Bruneaux G, Pickett LM, Bardi M, Payri R, Bazyn T (2012) Engine combustion network (ECN): characterization and comparison of boundary conditions for different combustion vessels. Atom Sprays 22(9):777–806

Naber JD, Siebers DL (1996) Effects of gas density and vaporization on penetration and dispersion of diesel sprays. SAE Trans 105:82–111

Otsu N (1979) A threshold selection method from gray-level histograms. IEEE Trans Syst Man Cybern 9(1):62–66

Pastor JV, García-Oliver JM, López JJ, Micó C (2016) Application of UV–visible light absorption and scattering technique to low absorption fuels under diesel-like conditions. Fuel 179:258–266

Payri R, Ruiz S, Salvador FJ, Gimeno J (2007) On the dependence of spray momentum flux in spray penetration: momentum flux packets penetration model. J Mech Sci Technol 21:1100–1111

Qi W, Zhang Y (2018) A three-color absorption/scattering imaging technique for simultaneous measurements on distributions of temperature and fuel concentration in a spray. Exp Fluids 59(4):70

Qi W, Zhang Y (2019) Quantitative measurement of binary-component fuel vapor distributions via laser absorption and scattering imaging. Appl Phys B 125(7):127

Qin W, Hung DLS, Xu M (2015) Investigation of the temporal evolution and spatial variation of in-cylinder engine fuel spray characteristics. Energy Convers Manag 98:430–439

Schulz C, Gronki J, Andersson S (2004) Measurements in a diesel spray. SAE tech paper 1032-1042

Senda J, Kanda T, Kobayashi M, Fujimoto H (1997) Quantitative analysis of fuel vapor concentration in diesel spray by exciplex fluorescence method. SAE tech paper 1012-1024

Vermorel O, Richard S, Colin O, Angelberger C, Benkenida A, Veynante D (2009) Towards the understanding of cyclic variability in a spark ignited engine using multi-cycle LES. Combust Flame 156:1525–1541

Westlye FR, Penney K, Ivarsson A, Pickett LM, Manin J, Skeen SA (2017) Diffuse back-illumination setup for high temporally resolved extinction imaging. Appl Opt 56:5028–5038

Wieske P, Wissel S, Grünefeld G, Graf M, Pischinger S (2006) Experimental investigation of the origin of cyclic fluctuations in a DISI engine by means of advanced laser induced exciplex fluorescence measurements. SAE tech paper 2006-01-3378

Wu S, Xu M, Hung DL, Li T, Pan H (2016) Analyzing the cycle-to-cycle variations of vapor and liquid phases of evaporating SIDI sprays via proper orthogonal decomposition technique. SAE Int J Engines 9(1):193–200

Yoon JK, Myong KJ, Senda J, Fujimoto H (2009) Analysis of spatial vapor-phase distribution using the LIF method on multi-component fuel. J Mech Sci Technol 23:2565–2573

Zhang Y (2001) A study on mixture formation in diesel sprays with split injection strategy. Dissertation, Hiroshima University

Zhang Y, Nishida K (2007) Vapor distribution measurement of higher and lower volatile components in an evaporating fuel spray via laser absorption scattering (LAS) technique. Combust Sci Technol 179:863–881

Zhang R, Sick V (2007) Multi-component fuel imaging in a spray-guided spark-ignition direct-injection engine. SAE tech paper 2007-01-1826

Zhang Y, Yoshizaki T, Nishida K (2000) Imaging of droplets and vapor distributions in a Diesel fuel spray by means of a laser absorption–scattering technique. Appl Opt 39:6221–6229

Zhang Y, Li S, Qi W, Nishida K (2017) Evaporation characterization of fuel spray impinging on a flat wall by laser-based measurement. Int J Engine Res 18:776–784

Zhou X, Li T, Lai Z, Wei Y (2019) Modeling diesel spray tip and tail penetrations after end-of-injection. Fuel 237:442–456

Zigan L, Schmitz I, Flügel A, Wensing M, Leipertz A (2011) Structure of evaporating single- and multicomponent fuel sprays for 2nd generation gasoline direct injection. Fuel 90:348–363

Zigan L, Shi JM, Krotow I, Schmitz I, Wensing M, Leipertz A (2013) Fuel property and fuel temperature effects on internal nozzle flow, atomization and cyclic spray fluctuations of a direct injection spark ignition-injector. Int J Engine Res 14:543–556

Affiliations

Wenyuan Qi[1] · Yifan Zhou[1] · Yuyin Zhang[1]

[1]   School of Mechanical Engineering, Shanghai Jiao Tong University, Shanghai 200240, China